Prediction of Variation in MIMO Channel Capacity for the Populated Indoor Environment Using a Radar Cross-Section-Based Pedestrian Model

Karla I. Ziri-Castro, William G. Scanlon, *Member, IEEE*, and Noel E. Evans

***Abstract*—Multipath propagation is a fundamental requirement for the operation of multiple-input multiple-output (MIMO) wireless systems. However, at ultrahigh frequency (UHF) and above, pedestrian movement may significantly affect the multipath propagation conditions in indoor environments. For the first time, a systematic analysis of the effect of pedestrian movement on channel capacity for an otherwise line-of-sight MIMO link in a single room is presented. A novel channel model for the populated indoor environment is also introduced, based on geometrical optics and a detailed radar cross-section representation of the human body. The new model generates a temporal profile for the complex transfer function of each antenna combination in the MIMO system in the presence of specified pedestrian movement. Channel capacity values derived from this data are important in terms of understanding the limitations and possibilities for MIMO systems. Capacity results are presented for a 42-m^2 single room environment, using a 2.45-GHz narrowband 8×8 MIMO array with 0.4λ element spacing. Although the model predicts significant increases in the peak channel capacity due to pedestrian movement, the improvement in mean capacity values was more modest. For the static empty room case, the channel capacity was 10.9 b/s/Hz, while the mean capacity under dynamic conditions was 12.3 b/s/Hz for four pedestrians, each moving at the same speed (0.5 m/s). The results presented suggest that practical MIMO systems must be sufficiently adaptive if they are to benefit from the capacity enhancement caused by pedestrian movement.**

***Index Terms*—Antenna arrays, channel capacity, diversity methods, fading, finite difference time domain (FDTD), modeling, multipath channels, multiple-input multiple-output (MIMO), radar cross section (RCS), radio propagation, ray tracing, simulation.**

I. Introduction

MANY future broadband wireless networks will feature dual spatial diversity with multielement arrays employed at both the originating and destination terminals. This multiple-input, multiple-output (MIMO) approach can yield significant gains for both link and network capacities, with no additional energy or bandwidth consumption when compared to conventional single-array diversity methods [1], [2]. The MIMO concept has attracted considerable interest both within academia and industry as an approach that can offer significant benefits for broadband wireless applications in future generation networks.

When a MIMO-based wireless communication system is deployed in suitably rich scattering conditions such as the indoor environment, a space-time coding architecture can be used to greatly increase the spectral efficiency of the system. At ultrahigh frequency (UHF) (300 MHz–3 GHz) and above, the indoor environment is ideal for MIMO systems as multipath propagation is almost assured. However, temporal channel variations may also occur due to the movement of personnel or, in industrial applications, vehicles, and equipment. Despite various measurement campaigns and a number of different approaches to MIMO channel characterization [3]–[5], the effect of scattering and blocking by pedestrians on indoor MIMO channel capacity has not yet been fully investigated. In this paper, a new deterministic propagation model is used to systematically analyze the temporal variation in theoretical channel capacity of a narrowband 2.45-GHz 8×8 MIMO system within a small room with pedestrian traffic. In addition, the new propagation model presented has wider applicability to the entire field of indoor propagation prediction.

The paper is organized as follows. Section II introduces the propagation model for populated indoor environments. The model is based on a combination of computational electromagnetic techniques: finite-difference time-domain (FDTD) modeling of transmitter and receiver arrays; image-based ray tracing; and detailed radar cross-section (RCS) modeling of a realistic human body phantom. Section III provides a theoretical overview of MIMO channel capacity and describes the technique used for converting the channel response matrix generated by the propagation model to a graphic representation of the dynamic MIMO channel capacity. Section IV presents simulation results for a single room environment under a variety of controlled conditions, including the empty room and up to four pedestrians. Section V draws conclusions from the work.

II. Propagation Model for Populated Environments

Human body shadowing is one of the factors that can significantly degrade transmission quality in indoor wireless systems [6]–[8]. Moving pedestrians can intersect the direct path of the wave between the transmitting and receiving antenna, potentially blocking the line-of-sight (LOS) path. Often, the communication link can be maintained by the contribution of reflected waves in the environment, as the propagation conditions become

Manuscript received July 18, 2003; revised December 23, 2003, April 1, 2004; accepted April 2, 2004. The editor coordinating the review of this paper and approving it for publication is A. Molisch.

K. I. Ziri-Castro and W. G. Scanlon are with the School of Electrical and Electronic Engineering, The Queen's University of Belfast, Belfast BT9 5AH, U.K. (e-mail: w.scanlon@qub.ac.uk).

N. E. Evans is with the School of Electrical and Mechanical Engineering, University of Ulster, Newtownabbey BT37 0QB, U.K.

Digital Object Identifier 10.1109/TWC.2005.846974

nonline-of-sight (NLOS). Another important source of variation in signal quality is the effect of reflections from the body itself. All biological tissues have a relatively high reflection coefficient at UHF and microwave frequencies. For example, taking the transverse electric case at 2.45 GHz, the minimum reflection coefficient $|\Gamma_{\mathrm{TE}}|$ for muscle is 0.775, assuming a relative permittivity of 52.7 and a conductivity of 1.74 S/m for the tissue. Doppler effects are not significant when considering pedestrian movement due to the low speeds involved: for example, even with a subject almost running, at 2 m/s, the resultant Doppler shift at 2.45 GHz is only 16.3 Hz, causing slow-fading effects. A more typical walking speed is around 0.5 m/s.

Overall, the effect on the propagation channel in populated indoor environments is time varying, dependent on the pedestrian traffic conditions, and related to the particular type of environment considered. Therefore, modeling channel variations caused by the relative positioning of pedestrians is important in the study of indoor wireless networks.

The propagation model presented in this paper is a new approach combining FDTD calculated bistatic RCS values for an anatomically realistic upright human body with conventional three-dimensional (3-D) image-based [9] geometrical optics. The result is a ray-tracing code that can include the effect of human bodies within the environment. The use of RCS is an improvement on previous attempts at modeling pedestrian effects [10], [11], where the human body was represented as a finite dielectric cylinder. However, it should be noted that the RCS approach is still only an approximation and, as with geometrical optics, becomes more accurate as the distances involved become larger with respect to the wavelength considered.

RCS can be considered as a measure of the target-created coupling between two antennas in free space [12] and embodies all possible wave interaction phenomena such as absorption, diffraction, reflection, and scattering. The RCS value for a target depends on frequency, target size, shape, composition, incident wave aspect, viewing aspect, and wave polarization. Once the RCS of a target $\alpha(\mathrm{m}^2)$ is obtained for these particular parameters the radar range equation can be written in terms of the power delivered by the receiving antenna to its load $P_r(\mathrm{W})$ s

$$P_r = \frac{P_t G_R G_T}{R_T R_R} \frac{\alpha}{4\pi R_T R_R} \left(\frac{\lambda}{4\pi}\right)^2 \tag{1}$$

where P_t is the transmitted power (W), R_R and R_T are the distances (m) from the target to the receiving and transmitting antennas, respectively, G_R and G_T are the antenna directional gains, and λ is the free space wavelength (m).

The ray tracing model operates as follows: all suitable paths from the transmitter to the receiver are determined using the image method, then the electric field strength and the phase for each ray reaching the receiver can be calculated. The total received power is obtained from

$$P_r = P_t \left(\frac{\lambda}{4\pi}\right)^2 \left| \sum_{i=0}^{N} \left(\frac{G_t(\phi_{ti}, \theta_{ti}) G_r(\phi_{ri}, \theta_{ri})}{d_i} \times \prod_{k=0}^{n_i<u} \Gamma_{k_i} e^{-j2\pi \frac{d_i}{\lambda}} \right) \right|^2 \tag{2}$$

where the directions of individual rays are specified by the θ_i and ϕ_i polar angles, d_i represents the total length of each ray, and n_i and Γ_{ki} are, respectively, the number of reflections and the kth reflection coefficient for the ith path. Only paths with a number of reflections lower than u are considered, where u is typically less than 5. N is the total number of paths added at the receiver point. For $i = 0$, (3) represents the contribution of the direct ray only, where it exists (in the LOS case). Since $\Gamma_{k0} = 0$, (2) becomes

$$P_{\mathrm{direct}} = P_t \left(\frac{\lambda}{4\pi}\right)^2 \left(\frac{G_t(\phi_{t0}, \theta_{t0}) G_r(\phi_{r0}, \theta_{r0})}{d_0}\right)^2. \tag{3}$$

All image-based ray contributions are checked for intersection with pedestrians, represented initially as 1.8-m high cylinders of 0.16-m radius. All geometrical optics rays, including the direct ray, that intersect bodies are considered "blocked" and are excluded from the summation process. However, the RCS contribution for each pedestrian in the environment is considered as an additional ray. The RCS value for the incident angle (transmitter position to the notional center of the cylinder representing the body volume) and outgoing angle (body to receiver position) is interpolated from a previously generated database.

The RCS database was produced using a brute-force technique where FDTD simulation (using the electromagnetic simulation software XFDTD 5.1[1]) of a realistic human body phantom was used for 664 discrete incoming angles. The body phantom represented a 109-kg 1.8-m-tall 39-year-old adult male standing upright and consisted of $157 \times 109 \times 396$ 5-mm cubic volume elements with six different tissue classifications. Tissue dielectric parameters were obtained from [13]. Each FDTD simulation was configured to generate a series of RCS values; these are frequency specific and the database needs to be specifically regenerated for each band of interest. A total of 7 941 240 individual RCS values were included in the database for 2.45 GHz: The mean value was -3.0 dBsm (0 dBsm $= 1\ \mathrm{m}^2$), and the logarithmic standard deviation was 17.3 dB. Fig. 1 shows an example plot for the azimuthal $(\theta_{\mathrm{out}} = 90^\circ)$ RCS response for the human body model with vertical polarization and an incidence angle of $\theta_{\mathrm{in}} = 55^\circ, \phi_{\mathrm{in}} = 90^\circ$. Note that the body is facing into the incident wave.

The propagation model presented earlier was validated at 2.45 GHz using a series of narrowband received power measurements obtained in a small rectangular room with floor dimensions 7 $\times$ 6 m and height 2.75 m. A 6.4-m point-to-point test link was established using an R&S SMIQ03B vector signal generator adjusted to deliver $+10$ dBm of continuous wave (CW) power to the transmit antenna's input port, taking account of feeder losses, and an Agilent E4407B spectrum analyzer was used to record received power at a sampling interval of 65 ms. The transmit and receive antennas (identical $+2.1$ dBi sleeve dipoles) were mounted at heights of 1.5 and 1.4 m, respectively. Fig. 2 shows the measured and simulated temporal received power profiles recorded as a pedestrian moved at 0.5 m/s perpendicular to the link's LOS path, midway between the antennas. Both measured and simulated profiles exhibited up to 4 dB of regular fading during LOS conditions, with significant

[1]Remcom Inc., Calder Sq., Box 10023, State College, PA 16805 USA.

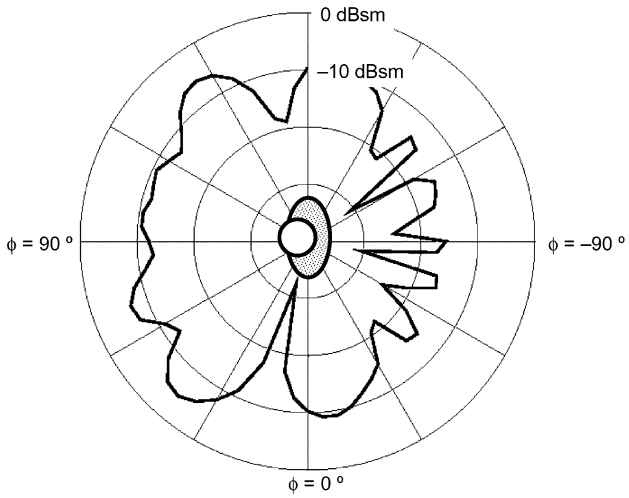

Fig. 1. Example plot of radar cross section in azimuth ($\theta_{\rm out} = 90°$) for the human body at 2.45 GHz. The incident field is vertically polarized with direction $\theta_{\rm in} = 55°$, $\phi_{\rm in} = 90°$, and the body is upright and facing into the wave.

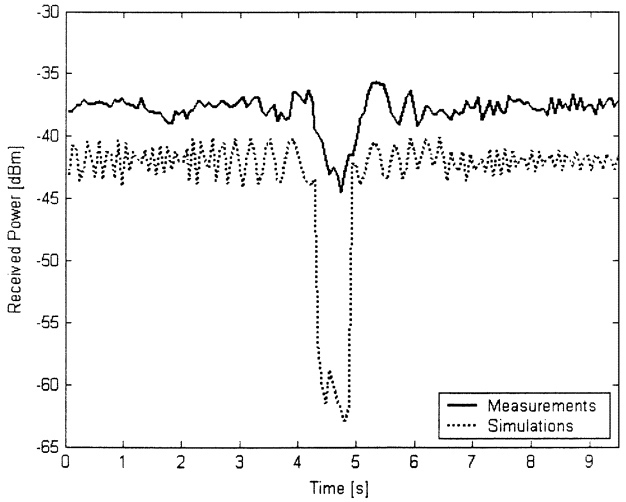

Fig. 2. Comparison of measured (with +10 dB vertical shift to aid readability) and simulated path loss at 2.45 GHz for a point-to-point link with a pedestrian crossing the direct ray.

attenuation occurring during the blocking (NLOS) phase. While in this example, the simulated blocking attenuation was higher than that measured, our measurements of similar links around 5 GHz have indicated up to 15 dB of attenuation for a single pedestrian obstruction [8]. The geometrical optics portion of the simulation code has also been successfully compared to extensive bodyworn terminal measurements in corridors and rooms at 5.2 GHz [14].

III. Modeling of MIMO Channels

A. Theoretical Capacity of MIMO Channels

It has been recently reported [15]–[17] that when MIMO systems are deployed in a suitably rich scattering environment there is considerable potential for obtaining high spectral efficiencies, provided that a suitable space-time code is used. If n antenna elements exist at each end of the link then it is possible to create n parallel channels between the transmitter and receiver elements, with a corresponding increase in spectral efficiency [18].

The full channel impulse response of a system, comprising of n_T transmit elements and n_R receive elements can, therefore, be described by an n_R-by-n_T complex matrix $\boldsymbol{g}(t,\tau)$, where each statistically independent and identically distributed element of $\boldsymbol{g}(t,\tau)$, $g_{ij}(t,\tau)$ represents the narrowband amplitude and phase response between each receive element i and each transmit element j, and the variables t and τ represent the delay and the clock time, respectively. $\boldsymbol{G}(t,f)$ is the Fourier transform of $\boldsymbol{g}(t,\tau)$. Considering the channel bandwidth as sufficiently narrow to treat its transmission characteristics as flat, the frequency dependence may be suppressed and the transform denoted as $\boldsymbol{G}(t)$. The following analysis considers $\boldsymbol{G}(t)$ at a fixed instant $t = t_0$, then for simplicity $\boldsymbol{G}(t_0) = \boldsymbol{G}$. It is also possible to define a normalized form of $\boldsymbol{G}$, as the matrix $\boldsymbol{H}$, where $\boldsymbol{H} = (\hat{\boldsymbol{P}}^{1/2}/\boldsymbol{P}^{1/2}) \cdot \boldsymbol{G}, \hat{\boldsymbol{P}}$ denotes the total transmitted power and $\boldsymbol{P}$ represents the average power at the output of each receiving antenna element [1]. The maximum possible capacity of the MIMO channel is then given by

$$C = \log_2\left[\det\left(\boldsymbol{I}_{n_R} + \frac{\rho}{n_T}\boldsymbol{H}\boldsymbol{H}^{\dagger}\right)\right] \text{ b/s/Hz} \tag{4}$$

where ρ is the average signal-to-noise ratio (SNR) at each receiver branch, I_{n_R} is the $n_R \times n_R$ identity matrix, det is the determinant, and $\{\cdot\}^{\dagger}$ represents the Hermitian transposition. $\boldsymbol{H}_{\rm ij}$ is normalized to remove the aggregate path loss component and only show the relative variation in the path responses between all $n_R \times n_T$ elements, assuming that they are statistically independent and gaussian distributed, as reported in [1], [19], and [20].

Using singular value decomposition, $\boldsymbol{H}$ can also be defined as

$$\boldsymbol{H} = \boldsymbol{U}\boldsymbol{D}\boldsymbol{V}^{\dagger} \tag{5}$$

where $\boldsymbol{U} \in \boldsymbol{C}^{n_R \times n_R}$ and $\boldsymbol{V} \in \boldsymbol{C}^{n_T \times n_T}$ are unitary matrices whose columns are the eigenvectors at the receiver and the transmitter, respectively. $\boldsymbol{D} \in \boldsymbol{C}^{n_R \times n_T}$ is a diagonal matrix whose diagonal elements are the positive square roots of the eigenvalues of $\boldsymbol{H}\boldsymbol{H}^{\dagger}, \lambda_i$ for $i = 1, 2, \ldots, n$ and $n = \min\{n_R, n_T\}$ [17]. The function $\min\{\cdot\}$ returns the minimum value of the arguments. Consequently, the multiplication of the unitary matrices $\boldsymbol{U}$ and $\boldsymbol{V}^{\dagger}$ transforms an $(n_R \times n_T)$ MIMO system into n single-input single-output (SISO) parallel channels with different power gains λ_i and uncorrelated fast fading statistics [20]. Equation (4) can then be rewritten as

$$C = \sum_{i=1}^{n} \log_2\left[1 + \frac{\rho}{n}\lambda_i\right] \text{ b/s/Hz.} \tag{6}$$

The absolute path power gains of each of these n parallel channels is given by the eigenvalues of the matrix $\boldsymbol{G}\boldsymbol{G}^{\dagger}, \sigma_i$ for $i = 1, 2, \ldots, n$. Similarly, the relative path power gains of each channel can be derived from the normalized channel matrix $\boldsymbol{H}$ as the eigenvalues of the channel matrix $\boldsymbol{H}\boldsymbol{H}^{\dagger}, \lambda_i$ for $i = 1, 2, \ldots, n$ [21].

TABLE I
PROPAGATION MODEL INPUT PARAMETERS

Parameter	Value
Carrier frequency	2.45 GHz
Maximum number of reflections considered	4
Number of antennas in each MIMO array	8
Antenna element spacing	0.4 λ
Transmitted power (per element)	–19.0 dBm
Relative permittivity of room walls	4.0
Conductivity of room walls	0.001 S/m
Relative permittivity of floor and ceiling	2.7
Conductivity of floor and ceiling	0.005 S/m

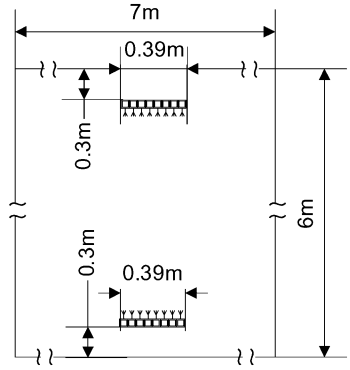

Fig. 3. Floor plan of the simulated environment.

B. Computational Process

The propagation model described in Section II was implemented using the ANSI-C programming language and configured to automatically produce the complex channel response matrix against time for the specified pedestrian traffic pattern. The program is capable of simulating 3-D room scenarios with both transmitting and receiving antenna arrays located inside. An unlimited number of pedestrians can be simulated within the room, each one with an individual speed and path. The image-based technique employed can be extended to include in-room objects such as doors, windows, and furniture. However, the focus of this study was to isolate pedestrian effects; the simulation of areas filled with additional, but stationary, clutter would have added unnecessary complexity to the analysis.

The simulation program receives text files describing all the required parameters as input, including pedestrian dimensions and trajectories, room dimensions, and electromagnetic parameters, location of MIMO arrays, antenna radiation patterns, and sampling rate. A separate 3-D radiation pattern is required for each antenna element in both transmit and receive arrays. Some of the constant parameters used in the simulations described in Section IV are presented in Table I. To calculate the absolute path power gains (σ_i) (the eigenvalues of matrix $\boldsymbol{GG}^{\dagger}$) of each of the eight SISO parallel channels, the MIMO and channel capacity (4) versus time, and to visualize the results, a set of MATLAB[2] functions were generated; these use the output matrix generated by the propagation simulator as their input and directly plot the results.

IV. SIMULATION RESULTS

A. Description of the Simulated Environments

The simulation scenarios considered in this work were all based on an 8×8 MIMO array fixed in position within a 7×6 m empty room (Fig. 3). A single room LOS environment was chosen as it presents worst-case conditions for MIMO operation and any changes in the channel response matrix caused by pedestrian movement will have a more dramatic effect on capacity. The transmit array was at a height of 1.95 m and the receive array was fixed 1.0 m above floor level. The location of the arrays within each room is also shown in Fig. 3. Both transmit and receive antennas were uniform linear arrays composed of eight vertically polarized $\lambda/2$ dipoles spaced at 0.4λ. The full 3-D radiation patterns for each individual dipole element were obtained by FDTD simulation and used as input to the propagation simulator. The peak antenna gain for both arrays was 3.7 dBi. One MIMO snapshot was recorded every 10 ms, with the total time simulated set to include all pedestrian movement (typically 13 s). The sampling interval of 10 ms represents a movement of 0.16λ at the maximum pedestrian speed and carrier frequency considered (2.0 m/s and 2.45 GHz, respectively); thus, the sampling interval is in accordance with the sampling theorem for the channel fluctuations caused by moving objects.

[2]The MathWorks, Inc., 3 Apple Hill Drive, Natick, MA 01760-2098 USA.

TABLE II
DESCRIPTION OF SIMULATION SCENARIOS

Scenario Reference	Number of pedestrians present	Description
0	*0*	Empty room
1NLOS	*1*	Static pedestrian
1A	*1*	Moving at 0.5 m/s
2A	*2*	Both moving at 0.5 m/s
2B	*2*	One at 1.0 m/s, one at 0.5 m/s
3A	*3*	All moving at 0.5 m/s
3B	*3*	1.0 m/s, 0.5 m/s, 0.39 m/s
4A	*4*	All moving at 0.5 m/s
4B	*4*	2.0 m/s, 0.66 m/s, 0.4 m/s, 0.29 m/s

The total transmit power for each simulation was -10 dBm, split over all 8 transmit elements (-19 dBm per element). The minimum distance between any two transmit and receive elements was 5.4 m and at 2.45 GHz, and the free space path loss is 54.8 dB. Ignoring all room reflections and pedestrian effects, the maximum received power at any one receive antenna due to the direct ray is ideally -66.4 dBm, taking into account maximum antenna gain at both ends of the link.

B. MIMO Channel Capacity Due to Pedestrian Movement

The situations simulated are denoted by a reference based on the number of pedestrians present, and where applicable, pedestrian speed. Table II provides a description for each of the nine scenarios and Fig. 4(a)–(e) illustrates the pedestrian locations and pathways. These particular simulations were chosen to represent the worst-case situations for MIMO systems where a strong LOS condition occurs. The presence of pedestrians then leads to two channel effects: LOS blocking and the formation

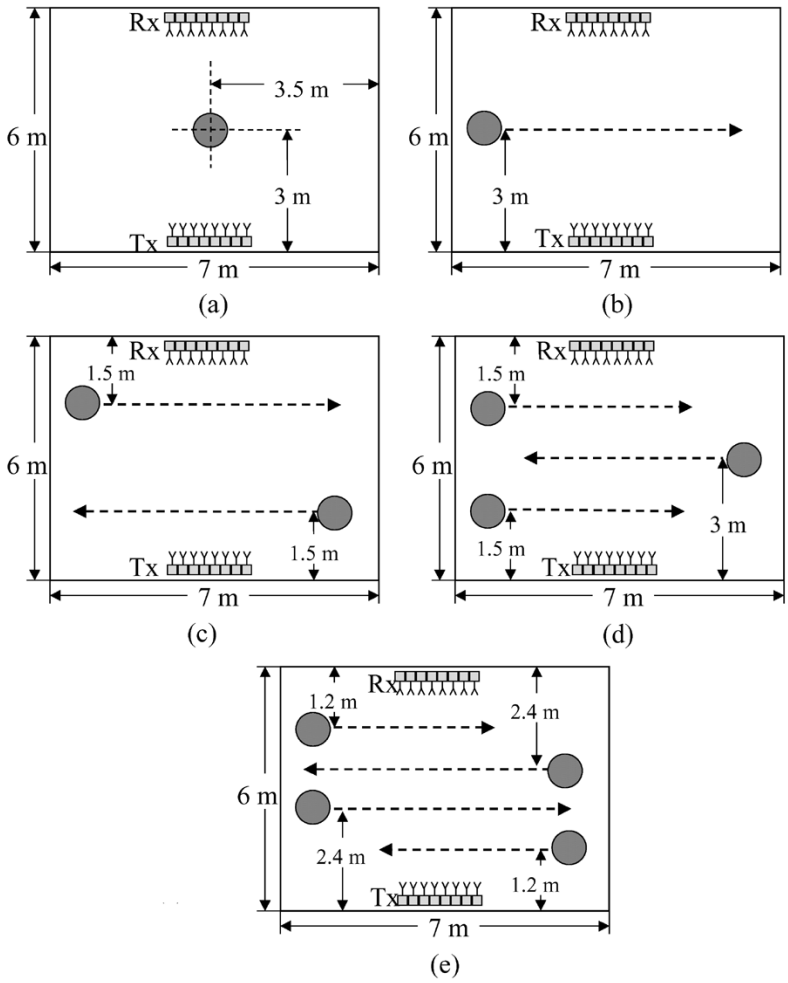

Fig. 4. Simulated scenarios (top view) for the pedestrian trajectories given in Table II. (a) 1NLOS. (b) 1A. (c) 2A and 2B. (d) 3A and 3B. (e) 4A and 4B.

of additional radiation paths due to body reflections. Overall results for received power and channel capacity are summarized in Tables III and IV, respectively. The mean received power was averaged over all time samples and all 64 transmit-receive antenna combinations. The mean dynamic range was calculated for all 64 time-series. The maximum dynamic range was the largest value recorded for any one of the 64 transmit-receive antenna combinations. The dynamic channel capacity profiles were computed using (4), the channel response matrix, and assuming, for each individual time step, a SNR value calculated from the average of the received power over all the 64 transmitter and receiver element combinations, with an average noise level of -83 dBm present at any receive element.

Scenario 0 is the baseline simulation of the empty room (without pedestrians). The mean received power for all of the 64 antenna combinations in this static scenario was -69.0 dBm/receive element. The static LOS channel capacity for this case was 10.9 b/s/Hz (SNR $= 14.0$ dB).

The effect of a single pedestrian standing upright in the center of the room and blocking the line of sight path was also simulated [Scenario 1NLOS, Fig. 4(a)]. Here, the average received power was reduced by 5.3 dB compared to the case without pedestrians and the corresponding channel capacity increased by 1.6 b/s/Hz to 12.5 b/s/Hz. In this case, the static pedestrian

TABLE III
SUMMARY OF RECEIVED POWER RESULTS AND DYNAMIC RANGE

Scenario Reference *(refer to Table II)*	Mean Received Power [dBm]	Dynamic Range [dB]	
		Mean	Max.
0	-69.0	0.0	7.5
1NLOS	-74.3	0.0	30.5
1A	-69.1	6.6	35.1
2A	-69.1	8.2	46.4
2B	-69.1	7.6	35.3
3A	-69.1	9.1	48.7
3B	-69.3	8.7	54.6
4A	-69.0	7.9	43.0
4B	-69.3	13.1	50.6

blocks the LOS for most of the transmit-receive antenna combinations, directly increasing the multipath scattering present in the environment. The MIMO channel capacity increased with the increase in the degree of decorrelation between the received signals [20], [21].

The effect of a single pedestrian moving at 0.5 m/s perpendicular to the link was then considered (Scenario 1A). The geometry [Fig. 4(b)] was such that a single NLOS event occurred during the temporal profile. Fig. 5(a) shows the received power profile averaged over all 64 possible combinations of transmit

TABLE IV
PEDESTRIAN DENSITY EFFECTS ON THEORETICAL MIMO CHANNEL CAPACITY

Scenario as per Figure 4	0	1NLOS	1A	2A	3A	4A	2B	3B	4B
Number of Pedestrians	0	1*	1	2	3	4	2	3	4
Maximum MIMO Capacity [bits/s/Hz]	10.9	12.5	14.1	14.7	16.7	17.8	14.2	15.0	16.1
Mean MIMO Capacity	10.9	12.5	11.2	11.3	11.9	12.3	11.6	11.9	12.4
10% MIMO Outage Capacity [bits/s/Hz]	10.9	12.5	9.9	10.2	11.2	11.0	11.0	10.8	11.4

* A single pedestrian standing upright in the center of the room, blocking the line of sight path.

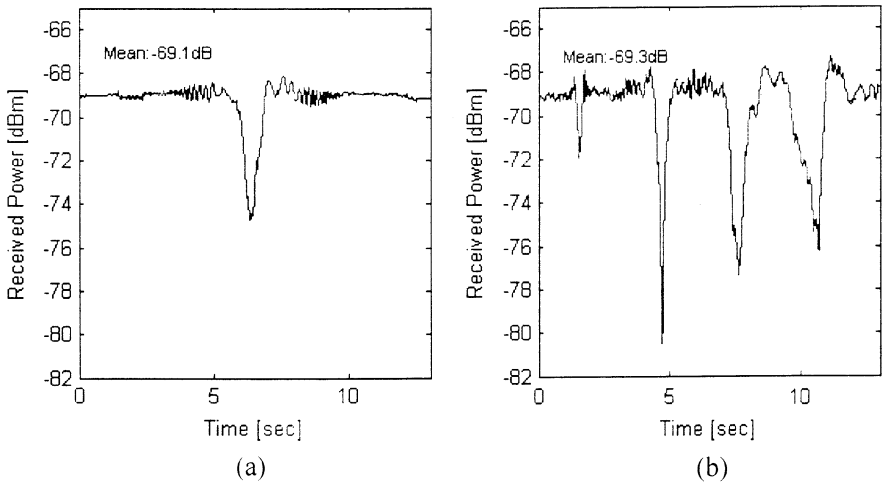

Fig. 5. Temporal profiles for received power, averaged over all the 64 transmitter and receiver combinations. (a) Scenario 1A. (b) Scenario 4B.

and receive antennas. Strong fading was observed in the region where the body obstructed the direct ray (at between 6 and 7 s); the average dynamic range over all the antenna combinations was 6.6 dB (Table III). However, some of the channels between individual transmit and receive elements varied over a dynamic range of up to 35.1 dB.

The duration of the NLOS fade in Scenario 1A was around 1 s, but would generally be dependent on the walker's speed. For example, Fig. 5(b) shows the element-averaged temporal received power profile for Scenario 4B [four pedestrians walking at different speeds, 2.0, 0.66, 0.4, and 0.29 m/s, respectively, transversally to the link with the geometry given in Fig. 4(e)]. The first fade occurs at 1.6 s, when the 2 m/s pedestrian obstructs the direct ray [Fig. 6(a)]. The next fade occurs at 4.8 s when the 0.7 m/s pedestrian obstructs the direct ray [Fig. 6(b)], and so on. The fade durations are directly proportional to pedestrian speed but it is also interesting to note that the four NLOS events present in Fig. 5(b) do not produce the same fade depth. Fig. 6(a)–(d) shows the relative positions of the pedestrians when each NLOS event occurs. The situations are not the same, as the fade depth is a function of direct ray attenuation, contributions from room reflections and individual pedestrian effects, including off-body reflections. For example, during the first fade, there is only one pedestrian partially blocking the line-of-sight, and additional reflections are present due to the positions of the other bodies.

The calculated temporal channel responses for this scenario are shown in Fig. 7. The dynamic SNR profile $\rho(t)$ [Fig. 7(a)] was calculated directly from the received power profile for this particular scenario [Fig. 5(a)]. Recently, it has been shown that variations in received SNR have a greater influence on the capacity of an indoor MIMO channel than do variations due to changes in the correlation of the channel response matrix [22], [24]. Therefore, the channel capacity results shown in Fig. 7(b) indicate that the partial NLOS event caused by the pedestrian introduces a capacity gain (peaking at 14.1 b/s/Hz) due to the enhanced role of the multipath components when only part of the receiver array is blocked. However, capacity is significantly reduced when total blocking occurs, due to the reduction in SNR.

An alternative view of the temporal MIMO channel variations can be obtained from the eigenvalues of $\boldsymbol{GG}^{\dagger}$, σ_i. Fig. 8(a) and (b) show the absolute path power gains of the eight SISO "parallel channels" for the scenarios with one pedestrian (1A) and four pedestrians (4B) described earlier. Fig. 8(a) shows that the variations in ρ [Fig. 7(a)] and, therefore, in capacity [Fig. 7(b)], caused by obstructive fading define the changes of the largest singular value of $\boldsymbol{GG}^{\dagger}$ [22], [23].

Fig. 9 shows the cumulative distribution functions (CDF) for the MIMO channel capacity time series as the number of pedestrians was increased from 1 to 4. Fig. 9(a) is for the scenarios with equal pedestrian speed (0.5 m/s), while the CDF in Fig. 9(b) is for those situations where each pedestrian

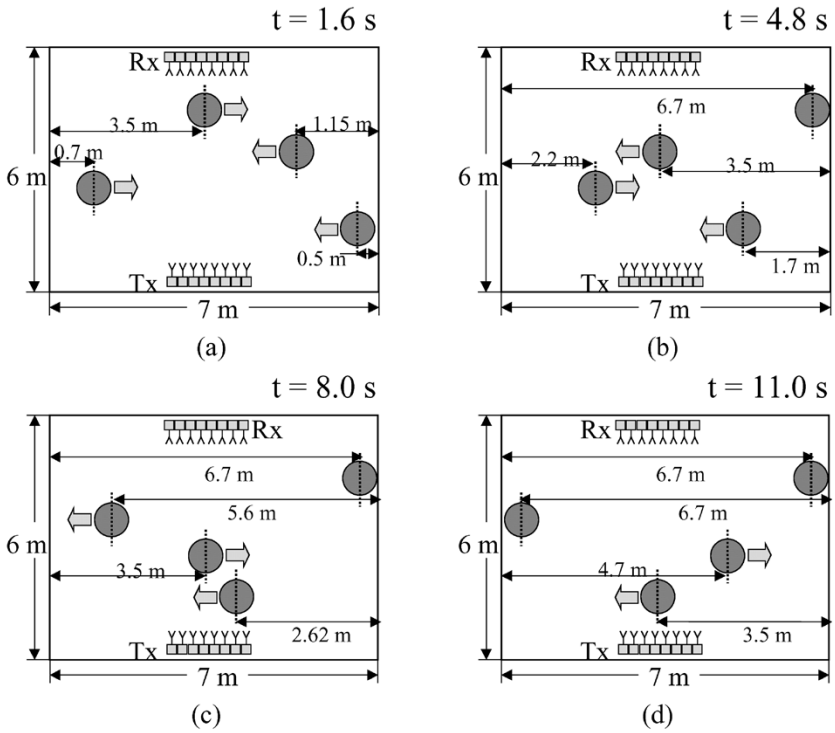

Fig. 6. Relative position of pedestrians for NLOS events in Scenario 4B at (a) 1.6, (b) 4.8, (c) 8, and (d) 11 s.

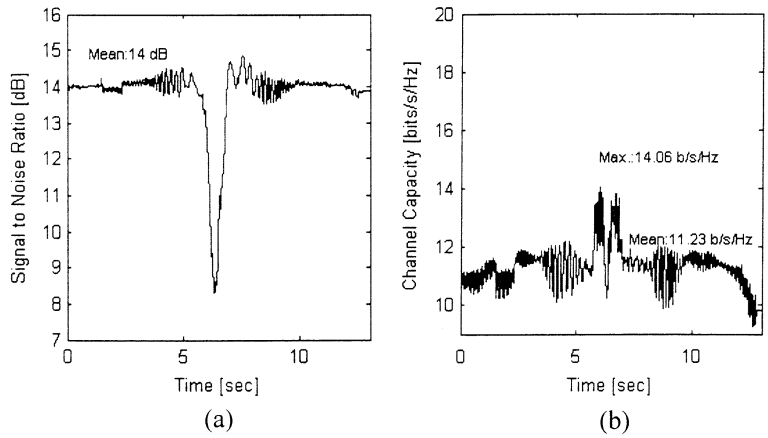

Fig. 7. Calculated channel performance for a single pedestrian walking at 0.5 m/s perpendicular to the link [Scenario 1A—shown in Fig. 4(b)]. (a) SNR averaged over all antenna elements at each time-step $\rho(t)$. (b) MIMO channel capacity $C(t)$.

is moving at a different speed. These CDFs demonstrate that channel capacity tends to increase with the number of pedestrians present. Furthermore, the results indicate that the MIMO channel capacity will fluctuate as the propagation conditions change in response to pedestrian movement. Therefore, for populated environments, adaptive MIMO schemes may be able to utilize the dynamic channel conditions caused by the continuously changing scatterer positions to achieve capacity enhancement.

The CDFs shown in Fig. 9 may also be used to estimate MIMO outage capacity. Table IV summarizes the mean and maximum MIMO channel capacity, and the 10% outage capacities, as a function of the number of pedestrians moving within the room. Fig. 10 shows the results for the scenarios where each pedestrian has a different speed (i.e., scenarios 2B, 3B, and 4B). Although the slopes of the responses are different, both mean and maximum channel capacity values increase monotonically with increasing scatterer density (i.e., from zero to four pedestrians present). However, for a higher number of scatterers, the maximum MIMO channel capacity might be asymptotically upper bounded, as reported in [25], where it was shown that this upper bound consists of the capacity of an identity channel of dimension equal to the number of scatterers.

V. Conclusion

For the first time, the effect of nearby pedestrian traffic on the channel capacity of a point-to-point indoor MIMO system was modeled, using an RCS-based propagation prediction tool for the populated environment. From the study of a single room

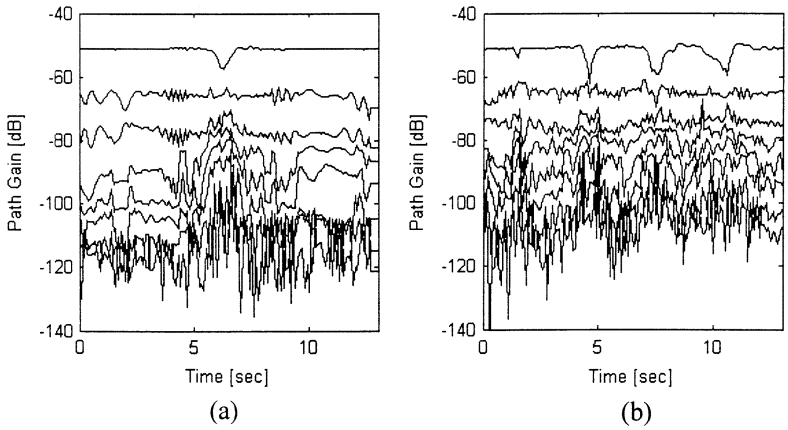

Fig. 8. Dynamic variation in the absolute power gains of the eight SISO parallel channels σ_i, for $i = 1, \ldots, 8$. (a) Scenario 1A. (b) Scenario 4B.

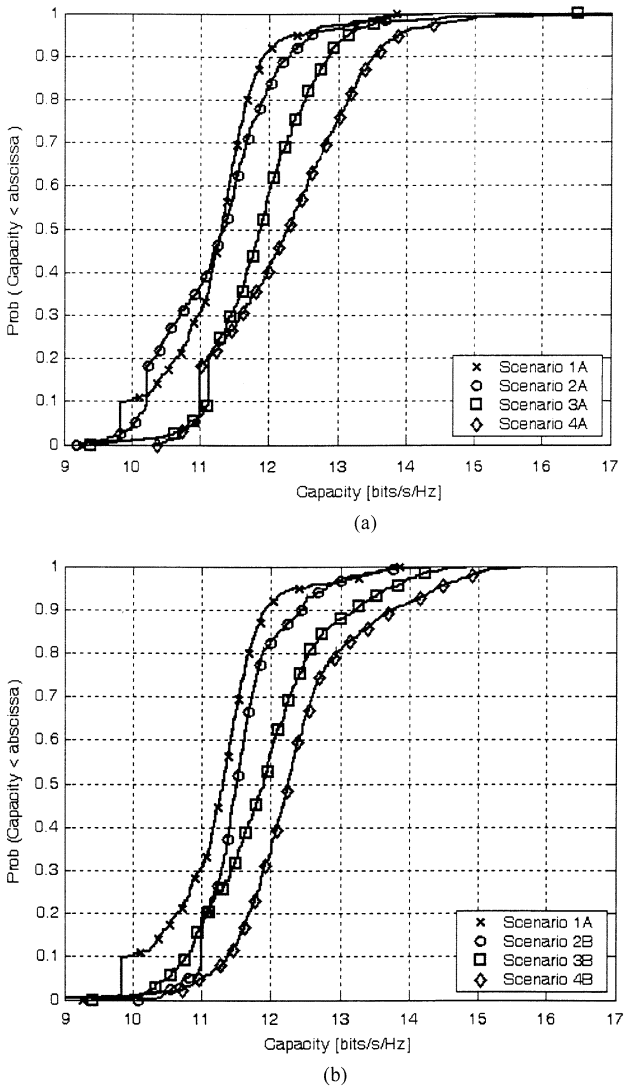

Fig. 9. Empirical CDF of the MIMO channel under the pedestrian movement conditions described in Table II. (a) For scenarios with all pedestrians moving at 0.5 m/s.(b) For scenarios with pedestrians moving at different speeds, with the single pedestrian case shown for comparison (Scenario 1A).

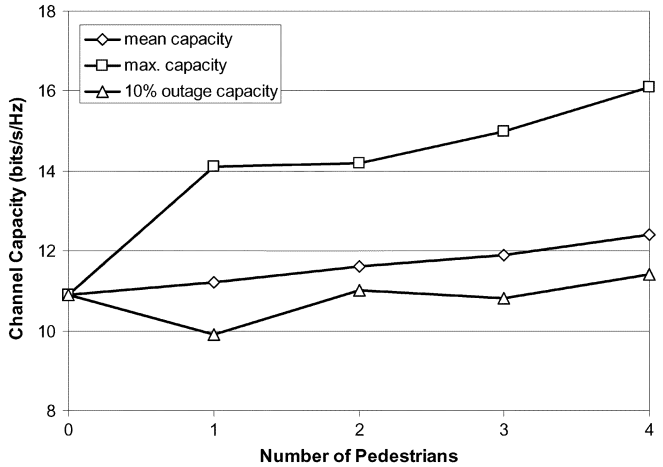

Fig. 10. MIMO channel capacity versus the number of pedestrians within the room, for scenarios with pedestrians moving at different speeds (ρ variable).

with up to four pedestrians, the results presented demonstrate that pedestrian effects significantly affect the theoretical maximum channel capacity of indoor MIMO systems. The mean channel capacity increased linearly with the number of pedestrians present within the indoor environment. With four pedestrians, the mean channel capacity rose by a maximum of 14% of the empty-room value. However, during total blocking caused by pedestrian movement, the consequential decrease in SNR leads to a reduction in channel capacity for the duration of the event. This is illustrated through the 10% outage capacity results, where the value for one pedestrian was less than that obtained for the empty room. Therefore, it is important to consider the dynamic value of SNR when determining the effect of moving scatterers such as pedestrians on MIMO channel capacity. Furthermore, there is a need for adaptive coding schemes to make best use of the dynamic fluctuations in available channel capacity in populated indoor environments.

Future effort should be directed at the analysis of different types of environment and pedestrian traffic conditions, including corridors and larger populated areas such as malls. In addition, the modeling technique described here could be directly applied to slow moving MIMO terminals, where the analysis should focus on the combination of multipath fading caused by the array moving in the environment and the effect of pedestrians.

REFERENCES

[1] G. J. Foschini and M. J. Gans, "On limits of wireless communications in a fading environment when using multiple antennas," *Wireless Personal Commun.*, vol. 6, no. 3, pp. 311–335, 1998.

[2] C.-N. Chuah, J. M. Kahn, and D. Tse, "Capacity of multi-antenna array systems in indoor wireless environment," in *Proc. IEEE GLOBECOM*, vol. 4, Sydney, Australia, 1998, pp. 1894–1899.

[3] Y. Kai, M. Bengtsson, B. Ottersten, D. McNamara, P. Karlsson, and M. D. Beach, "Second-order statistics of NLOS indoor MIMO channels based on 5.2 GHz measurements," in *Proc. IEEE GLOBECOM*, vol. 1, San Antonio, TX, 2001, pp. 156–160.

[4] T. Svantesson and J. Wallace, "Statistical characterization of the indoor MIMO channel based on LOS/NLOS measurements," in *Conf. Rec. 36th IEEE Asilomar. Conf. Signals, Systems, Computers*, vol. 2, Pacific Grove, CA, 2002, pp. 1354–1358.

[5] D. P. McNamara, M. A. Beach, and P. N. Fletcher, "Spatial correlation in indoor MIMO channels," in *Proc. 13th IEEE Int. Symp. Personal, Indoor, Mobile Radio Communications*, vol. 1, Lisbon, Portugal, 2002, pp. 290–294.

[6] S. Obayashi and J. Zander, "A body-shadowing model for indoor radio communication environments," *IEEE Trans. Antennas Propag.*, vol. 46, no. 6, pp. 920–927, Jun. 1998.

[7] K. Sato and T. Manabe, "Estimation of propagation-path visibility for indoor wireless LAN systems under shadowing condition by human bodies," in *Proc. 48th IEEE Vehicular Technology Conf.*, vol. 3, Ottawa, ON, Canada, 1998, pp. 2109–2113.

[8] K. I. Ziri-Castro, W. G. Scanlon, and N. E. Evans, "Measured pedestrian movement and bodyworn terminal effects for the indoor channel at 5.2 GHz," *Eur. Trans. Telecommun.*, vol. 14, no. 6, pp. 529–538, Nov./Dec. 2003.

[9] K. J. Gladstone and J. P. McGeehan, "Computer simulation of multipath fading in the land mobile radio environment," in *IEE Proc. Microw. Antennas Propag.*, 1980, pp. 323–330.

[10] F. Villanese, W. G. Scanlon, N. E. Evans, and E. Gambi, "A hybrid image/ray-shooting UHF radio propagation predictor for populated indoor environments," *Electron. Lett.*, vol. 35, no. 21, pp. 1804–1805, Oct. 1999.

[11] N. E. Evans, W. G. Scanlon, and F. Villanese, "Pedestrian-induced fading for indoor channels at 2.45, 5.7, and 62 GHz," in *Proc. 52nd IEEE Vehicular Technology Conf.*, vol. 1, Boston, MA, Sep. 2000, pp. 43–48.

[12] M. I. Skolnik, *Radar Handbook*. New York: McGraw-Hill, 1970.

[13] C. Gabriel, "Compilation of the dielectric properties of body tissues at RF and microwave frequencies," Brooks Air Force Base, Brooks AFB, TX, Tech. Rep. AL/OE-TR-1996-0037, 1996.

[14] K. I. Ziri-Castro, W. G. Scanlon, R. Feustle, and N. E. Evans, "Channel modeling and propagation measurements for a bodyworn 5.2 GHz terminal moving in the indoor environment," in *Proc. 12th IEE Int. Conf. Antennas Propagation*, vol. 1, Apr. 2003, pp. 67–70.

[15] D. W. Bliss, K. W. Forsythe, A. O. Hero, and A. L. Swindlehurst, "MIMO environmental capacity sensitivity," in *Conf. Rec. 34th IEEE Asilomar Conf. Signals, Systems, Computers*, vol. 1, Pacific Grove, CA, 2000, pp. 764–768.

[16] P. W. Wolniansky, G. J. Foschini, G. D. Golden, and R. A. Valenzuela, "V-BLAST: An architecture for realizing very high data rates over the rich-scattering wireless channel," in *Proc. Int. Symp. Signals, Systems, Electronics*, Pisa, Italy, 1998, pp. 295–300.

[17] J. Ling, D. Chizhik, and R. A. Valenzuela, "Predicting multi-element receive and transmit array capacity outdoors with ray tracing," in *Proc. IEEE Vehicular Technology Conf.*, vol. 1, Rhodes, Greece, 2001, pp. 392–394.

[18] J. P. Kermoal, P. E. Mogensen, S. H. Jensen, J. B. Andersen, F. Frederiksen, T. B. Sørensen, and K. I. Pedersen, "Experimental investigation of multipath richness for multi-element transmit and receive antenna arrays," in *Proc. IEEE Vehicular Technology Conf.*, vol. 3, Tokyo, Japan, 2000, pp. 2004–2008.

[19] C.-N. Chuah, G. J. Foschini, R. A. Valenzuela, D. Chizhik, J. Ling, and J. M. Kahn, "Capacity growth of multi-element arrays in indoor and outdoor wireless channels," in *Proc. IEEE Wireless Communications Networking Conf.*, vol. 3, Chicago, IL, 2000, pp. 1340–1344.

[20] D.-S. Shiu, G. J. Foschini, M. J. Gans, and J. M. Kahn, "Fading correlation and its effect on the capacity of multielement antenna systems," *IEEE Trans. Commun.*, vol. 48, no. 3, pp. 502–513, Mar. 2000.

[21] M. A. Beach, D. P. McNamara, P. N. Fletcher, and P. Karlsson, "MIMO—A solution for advanced wireless access?," in *Proc. 11th IEE Int. Conf. Antennas Propagation*, Manchester, U.K., 2001, pp. 231–235.

[22] D. P. McNamara, M. A. Beach, P. N. Fletcher, and P. Karlsson, "Temporal variation of multiple-input multiple-output (MIMO) channels in indoor environments," in *Proc. 11th IEE Int. Conf. Antennas and Propagation*, Manchester, U.K., 2001, pp. 578–582.

[23] J. B. Andersen, "Array gain and capacity for known random channels with multiple element arrays at both ends," *IEEE J. Sel. Areas Commun.*, vol. 18, no. 11, pp. 2172–2178, Nov. 2000.

[24] D. P. McNamara, M. A. Beach, P. N. Fletcher, and P. Karlsson, "Capacity variation of indoor multiple-input multiple-output channels," *Electron. Lett.*, vol. 36, no. 24, pp. 2037–2038, 2000.

[25] A. G. Burr, "Capacity bounds and estimates for the finite scatterers MIMO wireless channel," *IEEE J. Sel. Areas Commun.*, vol. 21, no. 5, pp. 812–818, Jun. 2003.

Karla I. Ziri-Castro received the degree in electrical and electronic engineering in 1998 from Simon Bolivar University, Caracas, Venezuela, and the Ph.D. degree from the Faculty of Engineering, Queen's University, Belfast, U.K., in 2004.

Her research interests include experimental and statistical characterization of microwave radio propagation within populated indoor environments.

William G. Scanlon (M'97) received the B.Eng. degree in engineering (first-class honors) and the Ph.D. degree for work on the numerical modeling of antenna-body interactions at radio frequencies from the University of Ulster, Coleraine, U.K., in 1994 and 1997, respectively.

He is currently a Senior Lecturer in telecommunications at Queen's University, Belfast, U.K. He has almost ten years of experience within the electrical and electronic industries, having worked for Nortel Networks, Monkstown, U.K., as a Senior RF Engineer and with Siemens U.K., Belfast, as a Project Engineer. His current research interests include antennas, radiowave propagation, bioelectromagnetics, wireless networks, and link layer protocols.

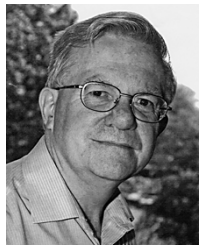

Noel E. Evans received the B.Sc. degree in electrical and electronics engineering, the M.Sc. degree in applied electronics, and the Ph.D. degree for work on programmable transversal filters built using intracell charge-coupled devices from The Queen's University of Belfast, U.K. in 1973, 1974, and 1977, respectively.

As a Senior Lecturer in the School of Electrical and Mechanical Engineering, the University of Ulster, Coleraine, U.K., he combines research interests in human and animal physiological signal acquisition using radio frequency techniques with the teaching of radio system theory and practice. His work, over 20 years in the area, has encompassed analogue circuit design for instrumentation, plus electromagnetic wave propagation studies from LF to UHF.